

Two-dimensional microlens arrays in silica-on-silicon planar lightwave circuit technology

Alexei L. Glebov
Lidu Huang
Shinegori Aoki
Michael G. Lee
Kishio Yokouchi
Fujitsu Laboratories of America
3811 Zanker Road
San Jose, California 95134
E-mail: aglebov@fla.fujitsu.com

Abstract. Two-dimensional (2-D) microlens arrays have been fabricated with silica-on-silicon planar lightwave circuit (PLC) technology. Several experimental techniques and computer simulation methods are applied to characterize properties of single and double microlens arrays, with one and two refracting surfaces, respectively. Systematic comparison of the measured and simulated beam propagation profiles enables optimization of the lens and module design resulting in higher input-output coupling efficiency. The insertion losses of the lens-slab-lens optical modules with 90-mm-long slab waveguides are measured to be 2.1 and 3.5 dB for the double and single lens modules, respectively. Comprehensive analysis reveals the major loss contributions. Excess losses of the modules caused by variations of the lens curvatures, material refractive indexes, light wavelength, etc., can be controlled within the acceptable limits. Further possibilities for the module loss reduction are discussed. Fairly weak wavelength dependence as well as overall stability of the module properties indicate that the microlens arrays are suitable for dense wavelength division multiplexing (DWDM) photonic networks. © 2003 Society of Photo-Optical Instrumentation Engineers. [DOI: 10.1117/1.1610481]

Subject terms: microlens array; planar lightwave circuit technology; silica on silicon; channel and slab waveguides; lens design; beam propagation profiles; beam propagation method; optical losses; wavelength dependence; optical switch; dense wavelength division multiplexing networks.

Paper 103003 received Jan. 31, 2003; revised manuscript received Apr. 30, 2003; accepted for publication May 16, 2003.

1 Introduction

In the recent decade, considerable attention has been given to the development of micro-optic lens arrays.¹ Due to keen interest in reducing dimensions of optical elements and systems as well as growing attempts to automate optical manufacturing, the development and fabrication of microlens arrays (MLAs) became a necessity. The arrays have found their applications in numerous areas of optics, fiber communications, and optical interconnects.²⁻⁴ However, with the advance of dense wavelength division multiplexing (DWDM) networks, the need for multichannel beam collimation and focusing grows steadily.^{5,6} For the most part, MLAs are built on a plane perpendicular to the light beam propagation with the refracting surfaces having 3-D profiles. Such 3-D MLAs are used in, for example, 3-D fiber array to fiber array connections, or 3-D optical switches with microelectromechanical systems (MEMS).^{3,6,7}

In the present work, 2-D light propagation in planar waveguiding structures receives primary consideration. Planar lightwave circuits (PLCs) already occupy a prominent place in telecommunication and data communication systems. Advantages and applications of planar integration have been reviewed plentifully in the technical literature.⁸⁻¹⁰ Monolithic and hybrid integration approaches have been developed for a number of active and passive networking devices, such as multiplexers/demultiplexers, filters, attenuators, transceivers, switches, etc.⁹⁻¹¹ The 2-D

and 3-D lightguiding structures can support low-loss transmission of confined lightmodes.^{8,12} Mostly single-mode channel waveguides are used in DWDM network devices. However, in some cases, it is necessary that collimated beams propagate rather long distances without confinement in the direction parallel to the surface and perpendicular to the beam propagation, i.e., slab waveguiding systems. Such devices require 2-D microlenses with slab waveguides that confine the light in the vertical direction and collimate or focus it in the lateral domain.

Figure 1 shows an example of such a device, namely an optical nonblocking cross-connect switch. The switch presented has only four channels. However, much higher channel count is certainly possible. The light signal enters and exits the device through the fiber arrays attached to the channel waveguides leading to the input MLA and from the output MLA. The input MLA collimates light into a beam that propagates through a slab waveguide, which can exceed a length of 100 mm. The output MLA focuses the incoming beam into the output channel waveguide. The input and output active elements, shown in the figure, can control the light beam propagation direction, for instance, enabling switching of the light beam from one output channel to another. The active elements may operate based on electro-optic, thermo-optic, acousto-optic, or any other principle allowing light beam deflection.¹³⁻¹⁶ The importance of MLA properties for the performance of devices, such as shown in Fig. 1, is quite obvious. In a previous

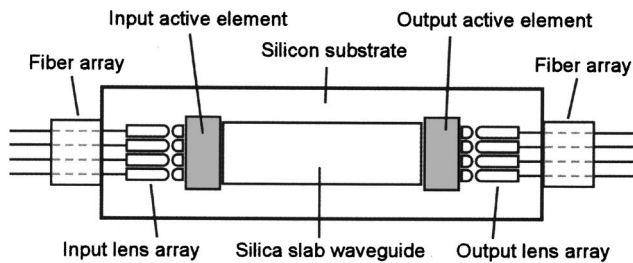


Fig. 1 A sketch of a nonblocking cross-connect optical switch built on a silicon substrate with planar silica microlens arrays, beam direction controlling active elements, and a slab waveguide.

study, Tsukamoto et al.¹⁷ demonstrated the feasibility of 2-D MLAs and discussed some design issues and properties of double lenses, pointing at their suitability for 2-D optical switches in photonic networks.

In the present work, two different types of planar MLAs are fabricated and their properties are studied in depth. Particular emphasis is placed on determining how different lens parameters as well as application conditions affect the performance of optical substrates with MLAs. Comparative analysis of the single and double lenses suggests preferential application conditions.

2 Lens Design

Single and double lenses represent the two different design types studied in the present work. Schematic drawings of both lens types are given in Fig. 2. A single lens shown on the top panel of the figure has one curved surface perpendicular to the substrate. In this case, the SiO_2/air interface refracts the light beam propagating in the lens along the substrate. A double lens, shown in the lower part of Fig. 2, has two curved surfaces, which face one another forming a double concave gap. The gap between the surfaces is filled with a polymeric material, which defines the light refracting interfaces $\text{SiO}_2/\text{polymer}$ and $\text{polymer}/\text{SiO}_2$. The refractive index (RI) of the filling material is lower than that of the lens. A lens design with a double convex gap and the RI of the gap filling material being higher than that of the lens is also possible. However, from the power loss point of

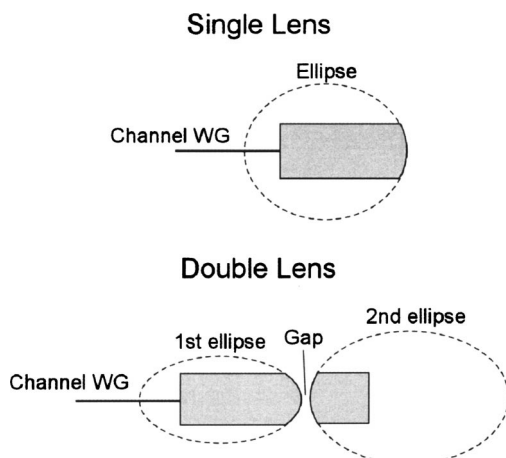


Fig. 2 Two types of microlenses. Top: a single lens with one elliptical surface. Bottom: a double lens with two elliptical surfaces.

Table 1 Design parameters of the lenses. The lens width is $575 \mu\text{m}$.

| | Major axis [μm] | Minor axis [μm] | Length [μm] | Focal length [μm] |
|----------|------------------------------|------------------------------|--------------------------|--------------------------------|
| | | Single lens | | |
| | 1148 | 833 | 2000 | 1938 |
| | | Double lens | | |
| 1st lens | 944 | 469 | 2000 | 1763 |
| 2nd lens | 2143 | 1066 | 450 | 4002 |

view, the concave gap is preferable, since it has the smallest gap size in the center of the lens, where the propagating light beam has the maximum intensity. In the gap, the light mode is no longer confined and diverges due to diffraction. Thus, minimizing the gap spacing at the position of the maximum intensity reduces the coupling loss. The double and single lenses discussed in this work represent only two possible cases for the lens gap design. The single lenses have the SiO_2/air refracting interfaces, i.e. maximized Δn , while the double lenses have $\text{SiO}_2/\text{polymer}$ refracting interfaces with minimized Δn and still practical lens curvatures. In fact, all intermediate cases of Δn are possible and are limited by the RI of the available index matching fluids (IMF).

Because of strong aberrations of spherical lenses, elliptical lens curvatures are designed, with two different ellipse dimensions for the first and second lenses of the double lens unit. Table 1 provides the exact dimensions of the microlenses tested in this work with the corresponding focal lengths. In contrast to a single lens, the output interface of a double lens is flat and, therefore, allows insertion of another IMF between the lens and the following optical element, for example, the active element in Fig. 1. This may reduce significantly the back-reflection losses and, thus, lead to a lower insertion loss (IL) of the device. The IMF in the gap between the lens and active element can be optimized to match the RI of the active elements and the silica waveguides.

Figure 3 depicts two types of optical modules tested in this work. The top and bottom panels show five-channel double and single lens strips, respectively. The incident beam enters the channel waveguide from a standard single-mode fiber on the left-hand side of the module, and then diverges to a specified width in the backside of the lens surface. The input lens collimates the beam, so that it can propagate efficiently through the following slab waveguide. The second MLA focuses the collimated beam and couples it into a channel waveguide for output. It is certainly possible to launch the incoming beam directly into the MLA without passing through the channel waveguides. The same is possible on the output side. Although this may reduce the total insertion loss of the module, the fiber-array alignment to the MLAs without channel waveguides becomes a highly complicated task and rather impractical, especially for the automated fiber array alignment.

3 Microlens Array Fabrication

Test MLAs have been fabricated using silica-on-silicon PLC technology at PLC foundry facilities. Details on stan-

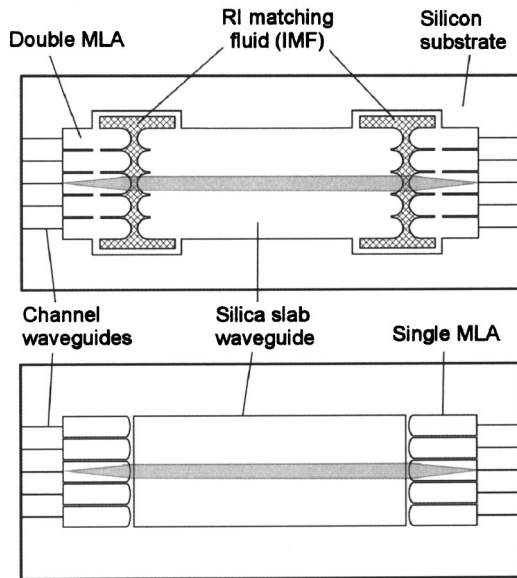


Fig. 3 Two types of optical lens-slab-lens modules integrated on Si substrates. Top: a double lens module. Bottom: a single lens module.

Standard PLC fabrication techniques can be found elsewhere.¹⁸ Separate MLAs as well as MLA modules with lenses on both sides and a silica slab waveguide in between, as those shown in Figs. 3(a) and 3(b), are manufactured on 6- and 8-in. silicon wafers. A three-layer stack consisting of the lower cladding, core, and upper cladding layers constitutes the planar lightguide for the vertical lightmode confinement. Thermal oxidation of the Si substrates forms the lower cladding layer, while chemical vapor deposition of P- and B-doped silica films forms the core and upper cladding layers. The thicknesses of the cladding and core layers are about 15 and 5 μm , respectively. The refractive index difference between the core and cladding layers is $\Delta n \sim 0.78\%$. The channel waveguides for the MLAs are formed with reactive ion etching (RIE). The width of the input channel waveguides is 5 μm for all modules, while the output channel waveguides are 5 and 45 μm wide. The length of the input channel waveguides is about 2 mm, whereas the length of the output channel waveguides is varied depending on the test. A deep RIE process, optimized for etching deep trenches in silica layers, is applied to form the gaps in the double lenses and trenches between the single lenses and slab waveguides.

An amorphous fluorocarbon polymer Cytop from Asahi Glass Company is filled in the double lens gaps. The Cytop RI is 1.333 at 1550 nm wavelength. The material is cured in a two-step process, with the preliminary cure at room temperature for 2 to 3 h and the final cure at 180°C for 60 min. For the insertion loss measurements, the input and output channel waveguides are polished on a polishing wheel to an optical quality, with a final surface roughness of less than 10 nm. The MLAs are separated from the slab waveguides for the beam-profile measurements.

Figure 4 shows SEM images of single Fig. 4(a) and double Fig. 4(b) lens arrays taken before the IMF filling in the lens gaps. A closer analysis reveals that the sidewall slope angles are in the range of 86 to 90 deg for all vertical

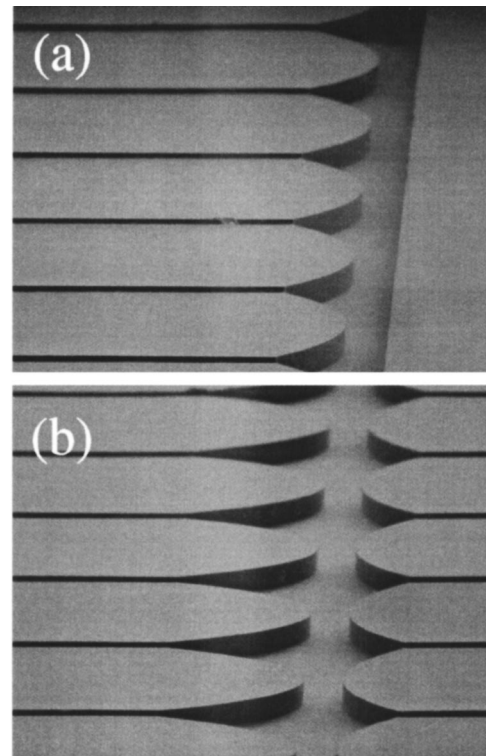


Fig. 4 SEM images of (a) single and (b) double microlens arrays.

walls across the wafer, with most of the walls having the slope angle higher than 87 deg. No significant sidewall roughness is visible in the SEM images. Only standard PLC manufacturing processes have been used for fabrication of the test modules presented in this work, which implies suitability of the process flow for mass production of optical substrates with 2-D collimating and focusing optics based on MLAs.

4 Lens Array Properties

This section describes various properties of the single and double lens arrays. The combination of experimental and theoretical methods provides access to numerous characteristics of the lenses and, thus, makes a thorough analysis of the MLA performance possible.

4.1 Experimental Techniques

Beam propagation profile measurements are conducted with a slit-based real-time beam profiler BeamScan® from Photon Incorporated. In this tool, a large-area monolithic detector collects light transmitted through a slit aperture as it passes through the beam. (Further information in regards to the measurement issues involved in scanning slit profilers can be found at www.photon-inc.com/appnotes.shtml.) This allows measurements of the profiles of the light beams propagating in the air. The beam width is measured at some specified percentage (clip level) of the peak amplitude. All presented profiles are measured at a clip level of 13.5% that corresponds to $1/e^2$. To measure a propagation profile, the scan head, placed on an automated rail, moves to the locations defined, and the peak profiles are recorded at each location. The propagation profiles presented below are

measured at a distance of 0 to 60 mm from the lens output with a measurement step of 5 mm. The beam width is then extracted from each profile after subtracting the background intensity. Each beam propagation profile measurement is repeated three times to avoid errors due to possible misalignment of the system. A final profile curve is averaged over these three measurements. All measurements are conducted in a semi-cleanroom facility with the ambient temperature control.

In addition, beam widths are measured after propagation in a 90-mm-long glass slab. The images of the output modes are captured with a CCD camera, and a peak analysis software package is used to extract the peak profiles with the corresponding beam widths. Unless specified, all measurements are conducted with a fiber optic laser source operating at 1550-nm wavelength. A tunable wavelength laser is employed for the wavelength-dependent measurements. In most cases, the output power is detected with an InGaAs semiconductor detector. To measure the power throughput of the optical modules shown in Fig. 3, optical fibers are aligned to the input and output channel waveguides of the modules using a semiautomatic fiber alignment tool with motorized micromanipulator stages.

4.2 Simulation Techniques

The lens design and optical module loss calculations are performed with a commercial optical analysis software package OptiBPM based on a beam propagation method (BPM). The 2-D BPM calculations combined with the effective index method are used to simulate the beam propagation profiles, which then can be compared to the profiles obtained experimentally. For the lens-slab-lens modules shown in Fig. 3, the input-output coupling efficiencies, not including the lens gap losses, can also be calculated using the 2-D BPM tool. The lightwave propagating in the waveguides is vertically confined everywhere in the module besides the lens gaps. Therefore, the 2-D tool provides quite accurate evaluation of the input-output coupling efficiency in the module, with the exception of the lens gap losses. In the 2-D BPM calculations presented next, the grid size and propagation step are $0.05 \mu\text{m}$. The lens gap losses are calculated separately.

The quasi-3-D and regular 3-D BPM methods provide estimates of the single and double lens gap losses. The later is straightforward, however, the computation of the complete, almost 100-mm-long module, is overwhelming, especially for wide planar waveguiding structures. To estimate the lens gap loss with the 3-D BPM method using reasonable computation resources, the length of the slab waveguide is reduced from 90 to 0.5 mm. The lens curvatures are optimized accordingly for the shortened slab waveguide. For this calculation, the grid size and propagation step are set to $0.2 \mu\text{m}$. The coupling efficiency (the device throughput) for the shortened double lens module is calculated to be 66% (1.805 dB), as derived from the signal power ratio at the output and input channel waveguides.

It is more effective to apply a quasi-3-D method to calculate the lens gap loss. The technique uses a 2-D BPM model with additional spatial integration. Figure 5(a) shows a vertical cross-section of a double lens unit. The light emerging from the first lens core propagates in free-space diverging on the way to the input of the second lens core

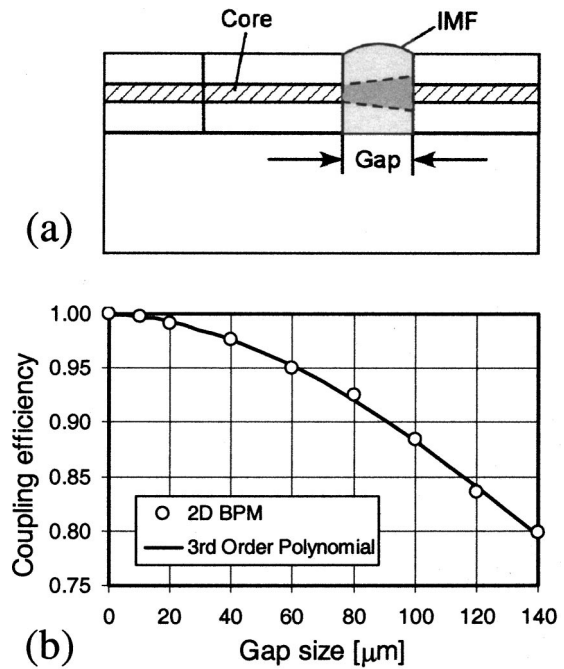


Fig. 5 (a) Vertical cross-section of a double lens showing the lens gap filled with index-matching fluid (IMF). (b) Lightmode coupling efficiency in the double lens as a function of the gap size.

layer. The gap between two lens surfaces is filled with IMF. The coupling efficiency in the vertical cross-sectional plane (i.e., between two slab waveguides) can be calculated with the 2-D BPM method. Figure 5(b) depicts the resultant 2-D coupling efficiency as a function of the gap size. The figure also shows a third order polynomial fitted to the BPM results, which is used in the integration described later.

The top view of a double lens is presented in Fig. 6. Due to the lens curvatures, the gap size is a function of the x coordinate. The “tip gap” is the gap size at the closest point between the lenses in the double lens unit. Taking into consideration the lens curvatures and the light intensity distri-

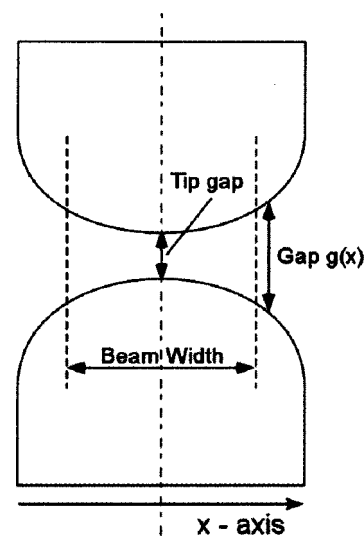


Fig. 6 Top view of a double lens.

bution along x , the lens gap loss may be calculated by integration over the cross-section area A perpendicular to the substrate and beam propagation direction. Before the wave front enters the lens region, the optical power can be expressed as

$$P_i = \int_A \frac{1}{2} \varepsilon(x,y) E(x,y)^2 dx dy,$$

where $\varepsilon(x,y)$ is the dielectric coefficient, and $E(x,y)$ is the electric field intensity. Assuming that the material is homogeneous allows rewriting of the equation to

$$P_i = \frac{1}{2} \varepsilon W_y \int_{\text{width}} E(x)^2 dx, \quad \text{where}$$

$$W_y = \int_{-h/2}^{h/2} \exp(-ay^2) dy,$$

a is the Gaussian coefficient, determined by a particular layer structure, and “width” is the beam width in x shown in Fig. 6. Similarly, the power after propagation through the lens can be expressed as

$$P_o = \frac{1}{2} \varepsilon W_y \int_{\text{width}} E(x)^2 \eta(g) dx,$$

in which the coupling efficiency $\eta(g)$ is shown in Fig. 5(b) and may be presented by an appropriate polynomial of the gap size $g(x)$. The lens gap loss is then calculated by

$$\begin{aligned} \text{Loss [dB]} &= -10 \log \frac{P_o}{P_i} \\ &= 10 \log \int_{\text{width}} E(x)^2 \eta(g) dx \\ &\quad - 10 \log \int_{\text{width}} E(x)^2 dx. \end{aligned}$$

A numerical integration procedure has been developed to evaluate the integrations. The results of the calculations are presented in Sec. 4.4.

4.3 Beam Propagation Profiles

In the optical modules shown in Fig. 3, the input MLA collimates the light beams exiting the channel waveguides, and the output MLA focuses the beams into the output channel waveguides. Between the lenses, the beams propagate in a slab waveguide, which may be up to 110 mm long. To minimize the total insertion loss of the system, the design of the input and output lenses should support the most appropriate beam propagation profiles. Thus, characterization of the beam propagation profiles as a function of lens design becomes one of the critical issues in developing low-loss 2-D optical systems with MLAs.

Arrays of single and double lenses with different lens curvatures have been fabricated. The minor axis of a single lens and the minor axis of the second lens in a double lens

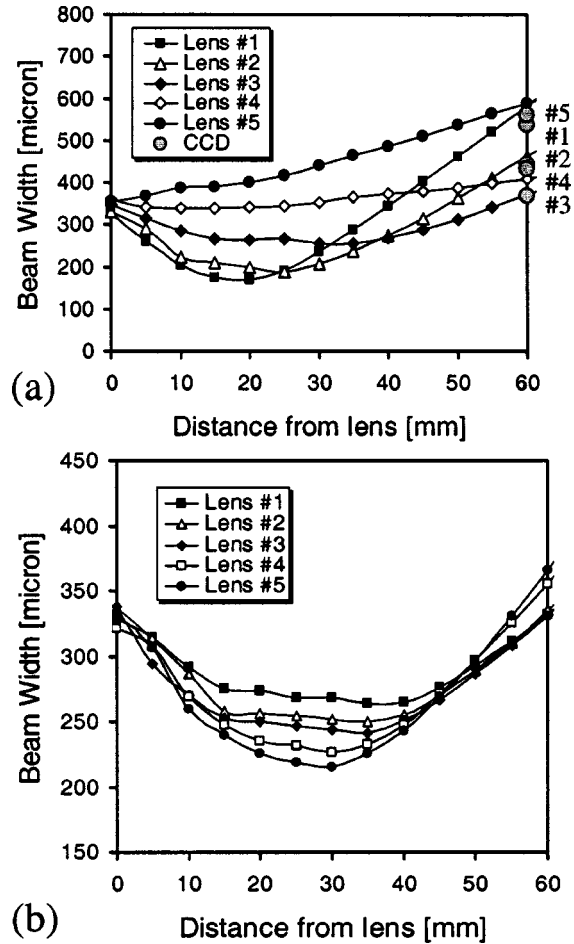


Fig. 7 Two sets of beam propagation profiles for different designs of the (a) single and (b) double lenses.

unit are varied with an increment of $5 \mu\text{m}$. Two sets of beam propagation profiles measured at 1550 nm are shown in Fig. 7(a) for the single lens and 7(b) for the double lens. In Fig. 7(a), lenses 1 and 5 have the smallest and largest minor axes, respectively. The design parameters for lens 3 are given in Table 1. It can be seen that the change of the single lens minor axis affects the propagation profiles rather strongly. Lens 3 offers the most symmetric profile with the beam width of about $250 \mu\text{m}$ at the Gaussian waist, and about $370 \mu\text{m}$ at 0 and 60 mm from the lens. Lenses 1 and 2 with smaller minor axes exhibit stronger cross-collimation that results in the beam width increase to about 550 and $450 \mu\text{m}$ at 60 mm from the lens, correspondingly. For the five single lenses measured, the output beam width changes by almost $200 \mu\text{m}$. The corresponding beam widths are also measured with a CCD camera at the output of a 90-mm-long glass slab. The results are plotted in Fig. 7(a) as round gray circles with the matching lens number.

Figure 7(b) presents the beam propagation profiles for five double lenses with different curvatures. Compared to the single lenses, the double lens profiles exhibit a significantly weaker dependence on the lens curvature. However, only the second lens minor axis is changed in this series.

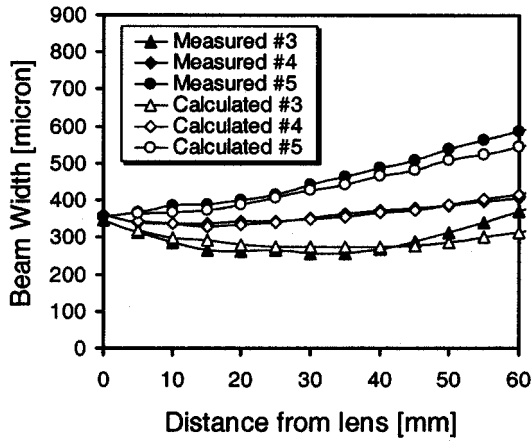


Fig. 8 Measured and calculated beam propagation profiles for three single lenses from Fig. 7(a).

The output beam width spread is less than 100 μm for the five double lenses tested.

The beam propagation profiles of selected lenses are also calculated with the 2-D BPM technique. As an example, the measured and calculated profiles for three single lenses are shown in Fig. 8. The good accord between the theory and measurements indicates that the 2-D BPM method can be applied with reasonably high accuracy for design and modeling of the planar optical systems with MLAs. Single lens 3 has been originally designed to provide the best propagation profile for the system. Figures 7(a) and 8 clearly demonstrate that the profile of lens 3 is the most symmetric and has the smallest beam width at the output. The effect of the lens curvature variations on the insertion losses of the lens-slab-lens modules shown in Fig. 3 is discussed in the following section.

4.4 Optical Module Losses

Insertion losses (IL) of the MLA modules shown in Fig. 3 with single and double lenses and 90-mm-long slab waveguides have been measured with the technique described in Sec. 4.1. Table 2 shows the results of the measurements for modules with 5- and 45-μm-wide output channel waveguides. The lowest loss of 2.1 and 3.5 dB are measured for the double and single lens modules, respectively. The data presented in the table are the channel-to-channel throughputs of the devices. The IL of the double lens module is lower than that of the single lens module by 1.4 and 1.9 dB, depending on the output channel width. In addition, the narrow output channel of 5 μm causes further losses of 1.5 and 2 dB in the double and single lens modules, respectively.

Table 2 Insertion losses of single and double lens modules with a 90-mm-long slab waveguide. The modules with 5- and 45-μm-wide output waveguides were tested.

| | 5 μm output | 45 μm output |
|-------------|-------------|--------------|
| Double lens | 3.6 dB | 2.1 dB |
| Single lens | 5.5 dB | 3.5 dB |

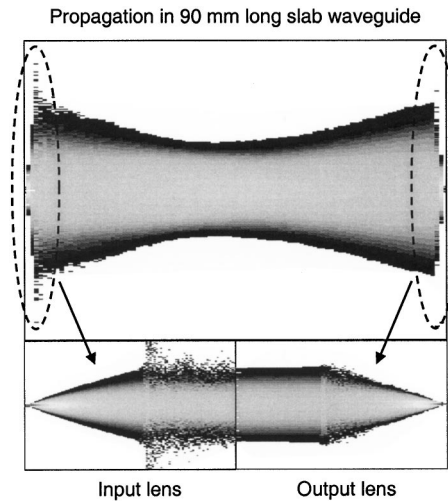


Fig. 9 Grayscale plot of the 2-D BPM results for the lens-slab-lens module with the double lens, with the design parameters given in Table 1.

The BPM loss calculations have been performed to understand the origin of the losses contributing to the IL of the modules. Figure 9 shows a grayscale plot of the 2-D BPM calculation results for the lens-slab-lens module presented in Fig. 3(b) with the parameters of double lens 3. The insets in the lower panel of the figure show the magnifications of the input and output sections of the module. As discussed in Sec. 4.2, the 2-D BPM technique provides a highly efficient tool to simulate 2-D beam propagation profiles as well as to evaluate the input-output coupling efficiencies, not including the lens gap losses. The lens gap losses can be evaluated with the quasi-3-D BPM method also described in Sec. 4.2. The calculation results of the coupling losses in the single and double lens gaps as a function of the gap size are given in Fig. 10. The gap size is 50 μm for both single and double MLAs in all modules tested. The losses caused by a 50-μm gap are calculated to be 0.55 and 0.8 dB for the double and single lenses, respectively.

The sidewalls of the lenses and slab waveguides are not perfectly vertical, as described in Sec. 3. This may cause some additional losses. The 2-D BPM method is used to

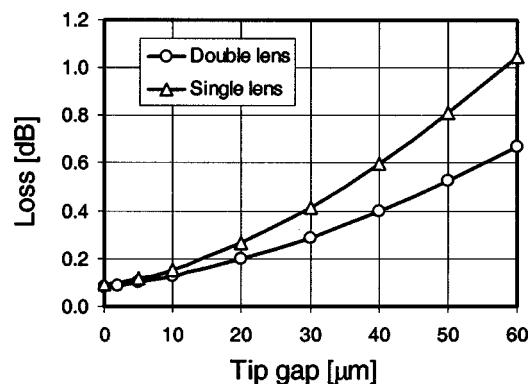


Fig. 10 Quasi-3-D calculations of the single and double lens gap losses as a function of the gap size.

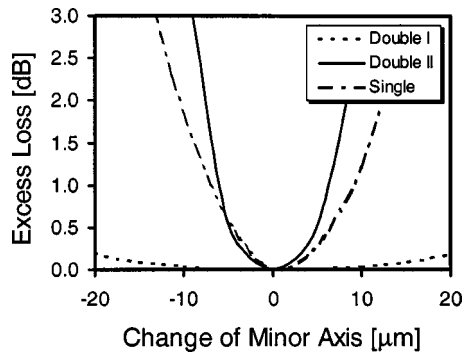


Fig. 11 Calculated excess losses in the MLA modules as function of the lens curvatures. “Single” means the minor axis of the single lens is changed; “Double 1” means the minor axis of the second lens in the double lens set is changed; and “Double 2” means both minor axis of the double lens are changed.

estimate the sidewall slope contributions to the lens losses. In the case of double lenses, this contribution is minimal, usually less than 0.1 to 0.2 dB, due to the interface RI matching with IMF. In the single lens case without IMF, the sidewall slope contribution can be as high as 0.2 to 0.3 dB per edge. Certainly the backreflections from the sidewall interfaces also have a very substantial contribution to the IL of the single lens module. In this case, each of the four interfaces may add up to 0.15 dB to the IL, as evaluated with the Fresnel’s equation.

PLC device processing can also lead to deviations of the lens dimensions from the designed values. The 2-D BPM method is used to calculate the excess losses caused by the lens minor axis variations. The length of the module for this evaluation is 110 mm. The results for the single and double lens modules are shown in Fig. 11. Note that the figure displays the excess losses, i.e., additional losses caused by the lens curvature variations. Thus, the lenses with the designed dimensions from Table 1 have obviously zero excess losses. The single curve in the figure is the result of the minor axis change of the single lens. The double 1 and double 2 curves are the results of the minor axis changes of the second lens and both lenses in the double lens unit, correspondingly. While the curve double 1 is quite flat, the curve double 2 is somewhat steeper than the curve for the single lens. Thus, if the curvature of the lens is changed from the designed value due to, e.g., overetch during deep trench patterning, the resulting excess

loss is somewhat smaller for the single lenses. In both cases, though, a deviation of the final curvature from the designed one by several microns can lead to excess losses of less than 0.1 to 0.2 dB.

Various effects, which may contribute to the IL of the single and double lens modules, are summarized in Table 3. Adding up the contributions easily accounts for the single and double lens IL difference experimentally determined (see Table 2). The origin of the higher loss of the modules with the 5- μm output channel waveguides is under investigation. This contribution might be reduced by fine tuning the full module design or by lateral tapering of the output channel waveguide. Further development is in progress.

The IL of 2.1 and 3.5 dB of the double and single lens modules, respectively, can be further lowered by decreasing the lens gap size, improvement of the sidewall profiles in the single lens modules, antireflective coatings of the interfaces, etc. For example, shrinking of the lens gap from 50 to 20 μm will result in the 0.6- and 1-dB loss reduction for the double and single lens modules, respectively.

4.5 Wavelength Dependence

The MLA wavelength independence is a very important property for potential applications of the modules in DWDM networks. The beam propagation profiles are measured in a range of wavelengths λ from 1460 to 1580 nm. The wavelength-induced excess losses are also calculated covering a wider range of λ .

The propagation profiles for the single and double lenses, with the design parameters listed in Table 1, are measured at different wavelengths and the results are shown in Figs. 12(a) and 12(b), respectively. Following the completion of different λ runs for a given lens, the profile at the original wavelength is remeasured to assure that no misalignment occurs during the run. The single lens profiles shown in Fig. 12(a) have very similar shapes for different λ , while the double lens profiles shown in Fig. 12(b) have obviously a noticeable change of the profile shapes. In the latter case the curves start crossing around 50 mm. A more accurate analysis of the beam profiles in the measured range of wavelengths demonstrates that the single lens beam width varies only by 10%, while the double lens beam width varies by up to 25% at a distance of 60 mm from the lens. Hence, the double lenses have stronger λ dependence than the single lenses. The λ dependence of the double lenses is mainly related to optical properties of the gap-filling material (Cytop in the present case) and, therefore, can be reduced by using different IMF.

The excess losses of the lens-slab-lens modules as a function of wavelength are calculated with the slab waveguide length of 110 mm. The results are displayed in Fig. 13. The figure shows the excess losses, not the IL, with the excess losses at the 1550-nm wavelength being zero. It should be noted that the calculation results for the double lenses are sensitive to the Cytop optical properties, which were not confirmed in this laboratory. For double lenses, the wavelength coefficient $\Delta n/d\lambda$ of the Cytop refractive index was estimated from the indexes measured at several wavelengths (from 238 to 546 nm, and at 1550 nm) as provided by the supplier. Therefore, the slope of the curve at 1550 nm could only be roughly estimated, which may

Table 3 Some contributions to the single and double lens module losses.

| | Parameter | Single lens | Double lens |
|----------------------|----------------------|-----------------|----------------|
| Material loss | ~100 mm | 0.5 to 1.0 dB | 0.5 to 1.0 dB |
| Curvature variations | 1 to 2 μm | <0.1 to 0.2 dB | <0.1 to 0.2 dB |
| Gap coupling | 50 μm | 2×0.8 dB | 2×0.55 dB |
| Back reflection | 4 interfaces | 4×0.15 dB | <0.05 dB |
| Sidewall slope | 4 interfaces | 4×0.1 to 0.2 dB | <0.2 dB |

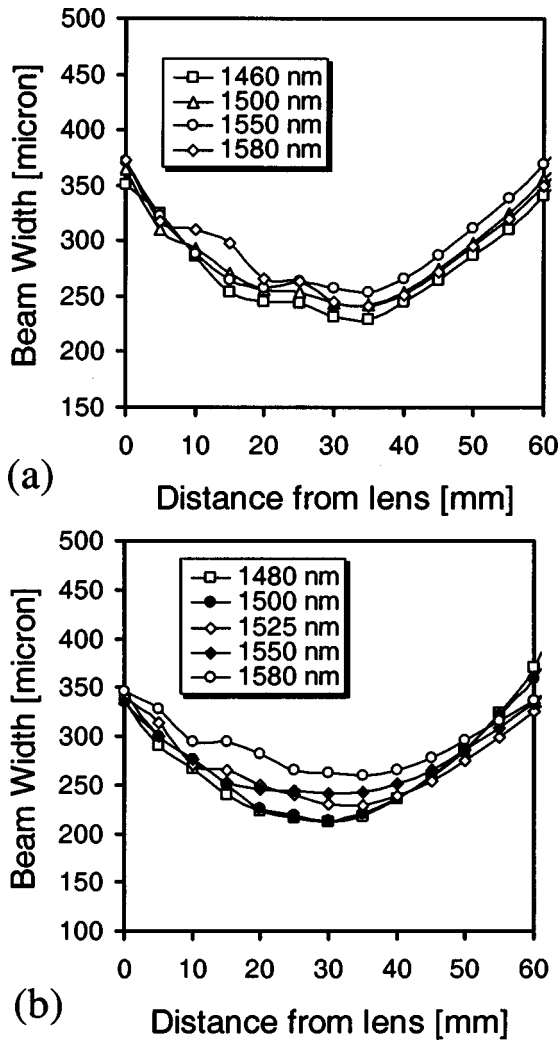


Fig. 12 Wavelength dependence of the beam propagation profiles for the (a) single and (b) double lenses.

cause an overestimate of the excess losses. The calculated curves also show that the λ dependence is significantly stronger for the double lenses. However, for the range of wavelengths from 1460 to 1580 nm, the excess loss absolute values do not exceed 0.1 dB in both cases. This weak λ dependence makes the experimental verification of the effect extremely difficult and also indicates that both lens types are suitable for application in DWDM photonic networks.

4.6 Material Refractive Index Variations

In MLA fabrication, some variations, of the lens material RI can be expected. The RI difference between the silica waveguide core and cladding layers Δn defines the numerical aperture of the lightguiding system, which can be slightly off from the specified value. Similarly, for the double lenses, the IMF RI can deviate from the specified value. In a well-established MLA fabrication process, these variations can be kept very small. Nevertheless, analysis of possible excess losses due to these variations is needed.

The calculated excess losses due to variation of the silica

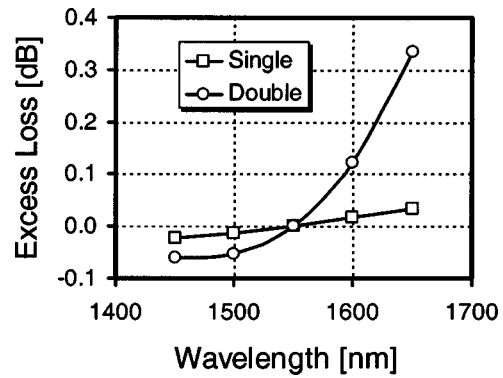


Fig. 13 Excess losses as a function of the light wavelength for the single and double lenses calculated with a 2-D BPM method. Zero excess loss is at $\lambda = 1550$ nm.

waveguide Δn are plotted in Fig. 14. The RI of the cladding layers and the double lens IMF is fixed at 1.444 and 1.333, respectively. The core layer index is varied from 1.4513 to 1.4593. The base design is performed for $\Delta n = 0.78\%$ and thus, the module with this value has no excess losses. Figure 14 shows that the single lens module has stable performance over a wide range of Δn . The double lens module is more sensitive to the Δn deviations. In standard silica-on-silicon PLC manufacturing, the core index deviation is usually less than 0.05% and, in most cases, is about $\pm 0.02\%$. In the range of the silica RI studied, both lens types exhibit excess losses substantially lower than 0.1 dB, thus indicating that this parameter has no significant effect on the MLA performance.

The RI of IMF filled in the double lens gaps may have stronger fluctuations due to temperature and time-dependent polymerization processes involved in the material curing. The effect of the IMF RI variations in the range from 1.330 to 1.336, or $\pm 0.25\%$, correspondingly, is simulated and the results are presented in Fig. 15. The measured Cytop RI is 1.333, which is the value used for the base design of the modules, and thus corresponds to zero excess losses. Figure 15 shows that deviation of the RI by 0.1% will result in the excess loss of less than 0.2 dB. Usually, it can be easily controlled to within 0.1% and, in fact, to a

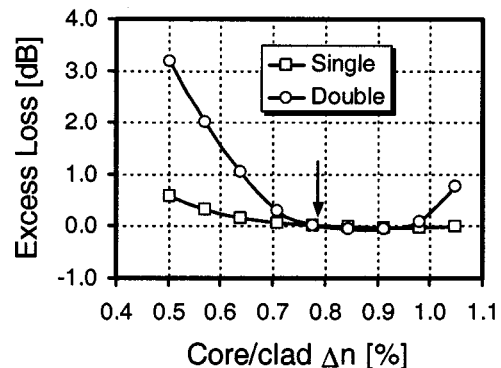


Fig. 14 Excess losses as a function of the RI difference Δn between the core and cladding layers. Zero excess loss is at $\Delta n = 0.78\%$.

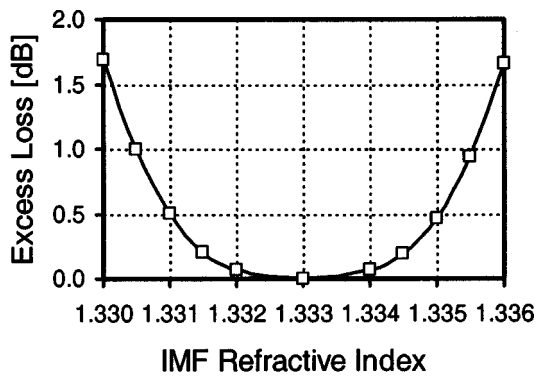


Fig. 15 Calculated excess losses for a double lens as a function of the IMF RI change.

significantly higher degree when the process is well established. Therefore, possible excess losses can be kept in the acceptable limits. Finally, it should be noted that many polymer IMFs have a rather strong thermo-optic effect. This might affect the performance of the MLA modules. Thus, all experiments reported in this work have been performed in a temperature-controlled environment. A study of temperature effects on the MLA module performance is underway.

5 Conclusions

Two types of planar MLAs, with single and double lenses, are fabricated using silica-on-silicon PLC technology. The microlenses have sidewall slopes better than 87 deg and show no substantial roughness detectable in the SEM. In addition to separate MLAs, single and double lens-slab-lens optical modules are fabricated, and their properties are studied with a number of experimental and theoretical methods.

The beam propagation profiles are measured for a series of lens designs and compared to the profiles calculated with a 2-D BPM method. The comparative study allows optimization of the lens designs. The resultant MLAs can collimate beams, which then can propagate through the slab waveguides up to 110 mm long, and have the output beam width less than 400 μm .

The insertion losses of the lens-slab-lens modules with 80-mm-long slab waveguides are measured for single and double MLAs. The double lens modules have the lowest losses of 2.1 dB. The single lens modules have losses of 3.5 dB. The simulations enable identification of the loss contributions. Among the most significant contributors to the IL are the lens gaps. A thorough evaluation of the gap losses for the single and double lenses reveals that a single lens module has about 1.1 dB higher losses just as a result of the gap divergence and backreflections.

The excess loss induced by the lens curvature variation imposed, e.g., by fabrication process biases, is slightly weaker for the single lenses. The measurements of the wavelength dependence of the beam propagation show that while the single lens profile shapes are rather unchanged, those of the double lenses change substantially. On the other hand, the excess loss calculations for the λ range of 1450 to 1600 nm demonstrate that the maximum loss pen-

alty is about 0.1 and 0.03 dB for the double and single lenses, correspondingly.

Effects of the material RI changes on the MLA performance are also evaluated. For single and double lenses, the excess losses are calculated as a function of Δn deviation from the designed value. Double lenses have somewhat higher Δn dependence, however, in both cases the excess losses do not exceed 0.5 dB for $\pm 0.1\%$ variations of Δn . Since the fabrication accuracy of Δn is usually on the scale of $\pm 0.02\%$, this can only cause additional losses of less than 0.1 dB. RI deviations of the index-matching fluid filling the double lens gap are also found to have a quite low effect on the total losses of the modules.

In conclusion, we demonstrate that both microlens types are suitable for DWDM network applications showing low sensitivity to processing conditions. The key advantage of the double lenses is potential reduction of the full device insertion losses by filling the index-matching fluid between all device interfaces. On the other hand, single lenses are less affected by variations of the lens curvature, light wavelength, and RI of the lens materials and, thus, have higher stability in the networks. In both cases, the fabrication processes are compatible with the majority of optical PLC facilities and are relatively simple and inexpensive, and thus can be employed for mass production of the integrated MLAs.

References

1. *Micro-Optics: Elements, Systems, and Applications*, H. P. Herzig, Ed., Taylor and Francis, Ltd. (1997).
2. K. Iga, "Semiconductor laser in the 21st century," *Proc. SPIE* **4277**, 11–25 (2001).
3. J. S. Leggatt and M. C. Hutley, "Microlens arrays for interconnection of single-mode fiber arrays," *Electron. Lett.* **27**, 238–240 (1991).
4. J. Jahns, "Planar packaging of free-space optical interconnects," *Proc. SPIE* **82**, 1623–1631 (1994).
5. Y. Tze-Wei, K. L. E. Law, and A. Goldenberg, "MEMS optical switches," *IEEE Commun. Mag.* **39**, 158–163 (2001).
6. D. J. Bishop, C. R. Giles, and G. P. Austin, "The Lucent LambdaRouter: MEMS technology of the future here today," *IEEE Commun. Mag.* **40**, 75–79 (2002).
7. P. B. Chu, S. S. Lee, and S. Park, "MEMS: The path to large optical crossconnects," *IEEE Commun. Mag.* **40**, 80–87 (2002).
8. Y. P. Li and C. H. Henry, "Silica-based optical integrated circuits," *IEEE Proc. Optoelectron.* **143**, 263–280 (1996).
9. T. Hashimoto and I. Ogawa, "Optical hybrid integration using planar lightwave circuit platform," *Proc. SPIE* **4652**, 58–67 (2002).
10. A. Himeno, "Silica-based planar lightwave circuits," *Mater. Res. Soc. Symp. Proc.* **597**, 41–50 (2000).
11. P. Kirsten and F. Bakhti, "Passive optical components for WDM-applications," *Proc. SPIE* **4277**, 54–68 (2001).
12. K. Okamoto, *Fundamentals of Optical Waveguides*, Academic Press, New York (2000).
13. Y. Chiu, R. S. Burton, D. D. Stancil, and T. E. Schlesinger, "Design and simulation of waveguide electrooptic beam deflectors," *J. Lightwave Technol.* **13**, 2049–2052 (1995).
14. C. H. Jang, L. Sun, J. H. Kim, X. Lu, G. Karve, R. T. Chen, and J. J. Maki, "A thin-film polymeric waveguide beam deflector based on thermo-optic effect," *IEEE Photonics Technol. Lett.* **13**, 490–492 (2001).
15. A. Kar-Roy and C. S. Tsai, "8×8 symmetric nonblocking integrated acoustooptic space switch module on LiNbO₃," *IEEE Photonics Technol. Lett.* **4**, 731–734 (1992).
16. M. G. Lee, S. Aoki, and K. Yokouchi, "High speed optical switch with prism deflector array," *IEEE/LEOS Annual Meeting Conf.*, Glasgow, Scotland, pp. 734–735 (2002).
17. K. Tsukamoto, A. Sugama, Y. Wakino, T. Miyashita, and M. Kato, "Simple microlens with polymer-filled trench in slab waveguide," *Fujitsu Sci. Tech. J.* **38**, 54–63 (2002).
18. *Silica Integrated Optical Circuits*, H. M. Presby, Ed., Sec. 2, "Fabrication," SPIE Milestone Series, Vol. MS 125, p. 43 (1996).



Alexei L. Glebov received his PhD degree in physics from the University of Goettingen, Germany, in 1997, and his MS degree in physics from the University of Saint Petersburg, Russia, in 1993. From 1998 until 2000 he worked at Bell Laboratories in Murray Hill, New Jersey, developing technologies for electronic and optoelectronic integrated circuits. In 2000 he joined the advanced optoelectronics technology department of Fujitsu Laboratories in San

Jose, California. His main research interests are planar lightwave circuit technologies, hybrid integration, and optical interconnects. He has published about 40 papers in refereed journals, participated in more than 30 conference presentations, and filed more than ten U.S. patents. He is a member of SPIE, IEEE, and MRS.



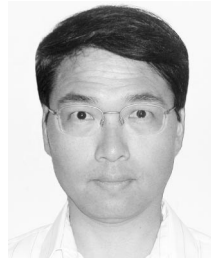
Lidu Huang received his BS degree in mechatronics in 1985 from Southeast University, and a MS degree in precision mechanical engineering in 1988 from Shanghai University, both in China. From 1988 to 1994, he was a lecturer at Shanghai University and a visiting scholar at Hong Kong Polytechnic University between 1990 and 1994. After received his PhD degree in mechanical engineering in 1997 from Rensselaer Polytechnic Institute, New York, he

worked on multiphysics analysis and MEMS optical component development at Texas Instruments, Incorporated, and Nanovation. He joined Fujitsu Labs in 2001 and has been developing optoelectronic components. He holds one patent and has authored or coauthored approximately 30 technical papers and conference presentations.



Shigenori Aoki received the BS degree in physics from Kyoto University, Japan, in 1985. In 1985, he joined the Materials and Material Engineering Laboratory of Fujitsu Laboratories Limited, Kanagawa, Japan, where he is engaged in research and development of packaging technology for high-speed microelectronics. Currently he is with Fujitsu Laboratories of America, where his research focuses on optoelectronics packaging. He is a member of the

IEEE-LEOS and SPIE.



Michael G. Lee received his PhD from University of Rochester, New York. He joined Fujitsu in 1991, and is currently working there as the Manager of the Advance Device Group. His areas of expertise are in optoelectronic devices, optical interconnection, and microelectronic packaging. His recent activities include optical backplanes, all-optical switches, high-density interposers, and multichip modules. He has 31 issued patents and more

than 30 publications.



Kishio Yokouchi received his ME degree in applied chemistry from Yokohama National University, Japan. In 1979, he joined the Materials Laboratories of Fujitsu Laboratories, Limited, in Japan, where he has been engaged in research and development of 8-in. 60-layer ceramic circuit boards, low-k polymer thin film circuit boards, high-density buildup circuit boards, polymer optical waveguide technologies, and liquid cooling systems for high-speed

servers. In 2000, he joined Fujitsu Laboratories of America, where he has been engaged in research and development of optical devices and interconnection technologies. He is a member of IEEE, OSA, and JIEP.